HHS Public Access

Author manuscript

Science. Author manuscript; available in PMC 2020 July 26.

Published in final edited form as:

Science. 2019 July 26; 365(6451): 386–392. doi:10.1126/science.aav3722.

Targeting a ceramide double bond improves insulin resistance and hepatic steatosis

Bhagirath Chaurasia[1,*], **Trevor S. Tippetts**[1,*], **Rafael Mayoral Monibas**[2,*], **Jinqi Liu**[2,*,†], **Ying Li**[1], **Liping Wang**[1], **Joseph L. Wilkerson**[1], **C. Rufus Sweeney**[1], **Renato Felipe Pereira**[3], **Doris Hissako Sumida**[3], **J. Alan Maschek**[4], **James E. Cox**[4], **Vincent Kaddai**[1], **Graeme Iain Lancaster**[5], **Monowarul Mobin Siddique**[6], **Annelise Poss**[1], **Mackenzie Pearson**[7], **Santhosh Satapati**[2], **Heather Zhou**[2], **David G. McLaren**[2], **Stephen F. Previs**[2], **Ying Chen**[2], **Ying Qian**[2], **Aleksandr Petrov**[2], **Margaret Wu**[2], **Xiaolan Shen**[2], **Jun Yao**[2], **Christian N. Nunes**[2], **Andrew D. Howard**[2], **Liangsu Wang**[2,‡], **Mark D. Erion**[2,§], **Jared Rutter**[4,8], **William L. Holland**[1], **David E. Kelley**[2,¶], **Scott A. Summers**[1,¶,#]

[1]Department of Nutrition and Integrative Physiology and the Diabetes and Metabolism Research Center, University of Utah, Salt Lake City, UT 84112, USA.

[2]Merck Research Laboratories, Merck, Kenilworth, NJ 07033, USA.

[3]School of Dentistry, São Paulo State University (UNESP), Araçatuba 16015, Brazil.

[4]Department of Biochemistry and the Diabetes and Metabolism Research Center, University of Utah, Salt Lake City, UT 84112, USA.

[5]Baker IDI Heart and Diabetes Institute, Melbourne, Victoria 3004, Australia.

[6]Faculty of Science, University of Brunei Darussalam, Gadong 1410, Brunei Darussalam.

[7]Sciex, Framingham, MA 01701, USA.

[8]Howard Hughes Medical Institute, Salt Lake City, UT 84112, USA.

Abstract

[#]Corresponding author: scott.a.summers@health.utah.edu.
[†]Present address: Bristol Myers Squibb, Princeton, NJ 08648, USA.
[‡]Present address: Morphic Therapeutic, Waltham, MA 02451, USA.
[§]Present address: Johnson and Johnson, Spring House, PA 19477, USA.

Author contributions: S.A.S., J.L., D.E.K., and B.C. conceived of the project, designed the experiments, and wrote the manuscript. B.C., T.S.T., R.M.M., J.L., Y.L., L.W., J.L.W., A.Po., C.R.S., R.F.P., V.K., G.I.L., M.M.S., S.S., H.Z., D.G.M., S.F.P., Y.C., Y.Q., A.Pe., M.W., X.S., J.Y., C.N.N., A.D.H.,L.W., M.D.E., D.H.S., J.R., and W.L.H. performed experiments and analyzed data. J.A.M., J.E.C., M.P. aided in lipid quantification.

[*]These authors contributed equally to this work.
[¶]These authors contributed equally to this work.

Competing interests: S.A.S. is a cofounder, J.R. is on the board of directors, and D.E.K. is a consultant of Centaurus Therapeutics. R.M.M., J.L., S.S., H.Z., D.G.M., S.F.P., Y.C., Y.Q., A.Pe., M.W.,X.S., J.Y., C.N.N., A.D.H., L.W., M.D.E., and D.E.K. are or were employees of Merck Research Laboratories.

Data and materials availability: *Degs1*$^{fl/fl}$ mice can be provided upon completion of a material transfer agreement to S.A.S. All data are available in the manuscript or the supplementary materials. RNA-seq data have been deposited in Gene Expression Omnibus under the accession number GSE132056.

SUPPLEMENTARY MATERIALS
science.sciencemag.org/content/365/6451/386/suppl/DC1

Ceramides contribute to the lipotoxicity that underlies diabetes, hepatic steatosis, and heart disease. By genetically engineering mice, we deleted the enzyme dihydroceramide desaturase 1 (DES1), which normally inserts a conserved double bond into the backbone of ceramides and other predominant sphingolipids. Ablation of DES1 from whole animals or tissue-specific deletion in the liver and/or adipose tissue resolved hepatic steatosis and insulin resistance in mice caused by leptin deficiency or obesogenic diets. Mechanistic studies revealed ceramide actions that promoted lipid uptake and storage and impaired glucose utilization, none of which could be recapitulated by (dihydro)ceramides that lacked the critical double bond. These studies suggest that inhibition of DES1 may provide a means of treating hepatic steatosis and metabolic disorders.

Sphingolipids such as ceramides and dihydroceramides are products of fat and protein metabolism that have been shown to accumulate in humans and nonhuman primates with obesity and hyperlipidemia (1–4). These lipids have been implicated in a wide range of cellular processes related to metabolism, growth, and survival (5, 6). Unbiased lipidomic screens in large clinical cohorts have revealed particularly robust associations between serum and tissue levels of ceramides and/or dihydroceramides and comorbidities of obesity, including insulin resistance, type 2 diabetes, and major adverse cardiac events (7–15). Some clinics have begun using serum ceramide levels as a measure of cardiovascular disease risk (7).

Ceramides and dihydroceramides consist of a sphingoid base coupled to a variable fatty acid side chain. They can be distinguished from one another by the presence (ceramides) or absence (dihydroceramides) of a 4,5-*trans* double bond in their sphingoid backbone (Fig. 1A) (5). Studies in purified systems reveal that this double bond alters the biophysical properties of the molecules, modifying their elastic properties and packing behavior (16). In most tissues, this double bond is inserted by the Δ4-desaturase activity of the enzyme dihydroceramide desaturase 1 (DES1), which is resident in the endoplasmic reticulum of virtually all cells. A second dihydroceramide desaturase isoform (DES2), which also has C-4 hydroxylase activity that enables it to produce phytoceramides that are important for barrier function, is present in tissues such as the skin, kidney, and intestines (5, 17). Both ceramides and dihydroceramides can serve as substrates for the enzymes that produce complex sphingolipids such as (dihydro)sphingomyelins and (dihydro)glucosylceramides (5, 18). The studies described herein investigated the role of these sphingolipids as causative agents in the development of insulin resistance and hepatic steatosis, which are major underlying causes of cardiometabolic disorders.

Experiments using cultured cells suggest that ceramides and dihydroceramides have distinct, nonoverlapping functions, particularly with regard to insulin action and apoptosis (1, 5). To investigate the effects of manipulations targeting the 4,5 double bond in ceramides on insulin resistance and hepatic steatosis, we generated gene-targeted mice by excising exon 2 of the *Degs1* gene (NP031879) encoding DES1. Specifically, we generated mice where exon 2 is flanked by LoxP sites, backcrossed them 10 times onto the C57BL/6 background, and bred them with mice expressing a tamoxifen-inducible Crerecombinase inserted into the *Rosa26* locus. The resultant conditional *Degs1* knockout mice (*Degs1*$^{Rosa26/ERT2\text{-}Cre}$) enable temporal control of gene depletion in a large number of tissues. *Degs1* removal led to an

increase in the proportion of sphingolipids lacking the 4,5 double bond in its sphingoid base (e.g., dihydroceramide and dihydrosphingomyelin) (fig. S1, A and B). Although we previously found that germline ablation of *Degs1* was lethal (19), removing it from adult animals produced no major health abnormalities or discernable signs of stress or discomfort. *Degs1* depletion reduced fat and liver mass, improved lipid and glucose handling (fig. S1, C to H), and elevated oxygen consumption (fig. S1K). No changes in respiratory exchange ratios, food intake, or ambulatory activity were observed (fig. S1, M to P).

We crossed these $Degs1^{Rosa26/ERT2\text{-}Cre}$ mice, as well as $Degs1^{fl/fl}$ littermates lacking *Cre*, with obese, leptin-deficient *ob/ob* mice that have impaired glucose tolerance and hepatic steatosis. At 20 weeks of age, we injected tamoxifen into the *ob/ob* $Degs1^{fl/fl}$ (control) and *ob/ob* $Degs1^{Rosa26/ERT2\text{-}Cre}$ offspring. The floxed allele from the *Cre*-containing strains was excised by administration of tamoxifen (Fig. 1B), which resulted in reduced ceramide/dihydroceramide ratios across a range of tissues (Fig. 1C and fig. S2, A to E). Other lipid classes, including glycerophospholipids (e.g., phosphatidylcholine, phosphatidylethanolamine, and phosphatidylserine), lysophospholipids, and sterols, were unaffected (fig. S2L). After *Degs1* ablation, animals displayed notable improvements in glucose and insulin tolerance (Fig. 1, G to J). *Degs1* depletion also halted weight gain in *ob/ob* mice by way of reduced fat mass (Fig. 1, D to F). Glucose and insulin tolerance tests were conducted before the onset of weight loss. *Degs1* deletion did not affect oxygen consumption (VO_2), carbon dioxide production (VCO_2), ambulatory activity, or food intake but modestly reduced respiratory exchange ratios (fig. S2, F to I). Histological assessment revealed that *Degs1* depletion resolved hepatic steatosis and decreased the size of adipocytes in the epididymal and subcutaneous adipose beds (Fig. 1K). No adipose browning was observed (fig. S2M). Circulating alanine transaminase (ALT) and aspartate transaminase (AST), which are measures of nonalcoholic fatty liver disease (steatohepatitis), were markedly reduced in the *ob/ob Degs1* knockouts (Fig. 1L). Thus, global *Degs1* depletion increased the proportion of sphingolipids lacking this conserved double bond and elicited a broad spectrum of metabolic benefits characterized by improvements in glucose and lipid handling.

To probe tissue-specific mechanisms that account for this phenotype, we selectively deleted *Degs1* from either the liver, adipose tissue, intestine, or myeloid cells. Although excising *Degs1* from intestinal or myeloid cells had no effect on any metabolic parameters assayed (figs. S8 and S9), *Degs1* removal from the liver and/or adipose tissue improved glucose and lipid handling (Fig. 2 and figs. S3 to S7). Specifically, we excised the gene from adipose tissue by crossing the $Degs1^{fl/fl}$ mice with mice expressing Cre recombinase under the control of the adiponectin promoter (20). *Degs1* was deleted in the liver by injecting adeno-associated virus expressing Cre recombinase (under the control of the human thyroid hormone–binding globulin promoter) into $Degs1^{fl/fl}$ mice. In a subset of animals, we deleted the genes from both adipose tissue and liver simultaneously. Although changes in transcripts were restricted to the targeted tissue (i.e., liver or adipose), ceramide/dihydroceramide ratios were altered in multiple locales, supporting our previous observation that these sphingolipids transmigrate between tissues (Fig. 2, A and B, and figs. S3, A to C; S4, A and B; S5, A and B; and S6, A to D) (20). Using a metabolomic flux assay to measure the rate of incorporation of a stable serine isotope into ceramides, we confirmed that rates of ceramide

production were substantially reduced in primary adipocytes isolated from the *Degs1*$^{\delta Adipo}$ mice (fig. S3C). All mouse strains were fed an obesogenic diet for 8 weeks before undergoing the metabolic phenotyping protocol. Gene depletion from either adipose tissue or the liver comparably improved glucose tolerance and decreased circulating levels of glucose (in fed and fasted mice), insulin, and fatty acids (Fig. 2, F to J). Depleting *Degs1* from either compartment decreased liver fat, with the effect of the liver-targeted deletion being more robust (fig. S6D), and decreased levels of several inflammatory cytokines (fig. S6C). Knockout and control animals exhibited comparable body and tissue mass, VO_2, VCO_2, energy expenditure, respiratory exchange ratios, food in-take, and ambulatory activity under both normal chow diet (NCD) and high-fat diet (HFD) feeding regimens (Fig. 2, C and E, and figs. S5, C to J, and S7, G to M). These findings suggest that the benefits caused by global *Degs1* depletion could result from separate actions in adipose tissue or the liver, independent of effects on weight gain or locomotor activity.

To further explore whether inhibition of DES1 may improve metabolic disorders, we delivered short hairpin RNAs (shRNAs) targeting the *Degs1* transcript to the liver of mice using adeno-associated viruses (AAVs). After screening 10 potential shRNA sequences (fig. S10A), we identified one (shRNA8) that produced strong *Degs1* knockdown in vitro and in vivo, substantially reducing the levels of liver ceramides (fig. S10, B and C). Having confirmed target engagement, we studied the effect of sustained *Degs1* knockdown on glucose homeostasis. In an intervention study, we generated diet-induced obese (DIO) mice by feeding 20-week-old C57BL/6 mice with an obesogenic HFD for 12 weeks. Mice were then injected with either low doses (1×10^{11} genome copies/mouse) or high doses (3×10^{11} genome copies/mouse) of AAVs expressing shRNA8 (AAV-*Degs1*) or a scrambled control (AAV-control). For comparison, we also conducted a prevention study by injecting the AAVs before starting the HFD feeding regimen. Twelve weeks after AAV administration, both low- and high-dose injections resulted in ~50% knockdown of *Degs1* mRNA in liver (Fig. 3A), suggesting sustained target engagement. Lipidomic analysis revealed that the shRNA reduced ceramide/dihydroceramide ratios in the liver, adipose tissue, and plasma but not in muscle (Fig. 3, B and K, and fig. S10, D and E). In the intervention protocol, knockdown of liver *Degs1* improved insulin sensitivity and glucose homeostasis (Fig. 3, D to H, and fig. S10F) without affecting body mass. Hyperinsulinemiceuglycemic clamp assessments revealed that the liver-restricted knockdown led to markedly improved whole-body insulin action, evidenced by the increased glucose infusion rate (GIR) needed to maintain euglycemia (Fig. 3I). The elevation in GIR caused by *Degs1* knockdown was attributed to both increased glucose disposal (Fig. 3I) and enhanced suppression of hepatic glucose production (Fig. 3J), indicating that liver-tropic *Degs1* knockdown improved both hepatic and non-hepatic insulin resistance. In the prevention protocol, AAV-*Degs1* elicited the same improvement in glucose homeostasis but also reduced weight gain (Fig. 3, L to O). This latter effect on body habitus occurred independent of food intake (Fig. 3M), thus recapitulating the effect seen after ablation of the *Degs1* gene in the *Degs1*$^{\delta Liver}$ animals.

These findings from *Degs1* knockout mice suggest that ceramides induce selective insulin resistance (21), a term previously reported to describe a prediabetic condition characterized by defective insulin action toward glucose metabolism (i.e., increased gluconeogenesis in liver and impaired glucose uptake in muscle and adipose tissue) coupled with an apparent

lack of insulin resistance toward lipids (i.e., enhanced triglyceride production). The disruptive effects of ceramide on glucose homeostasis are attributable to its inhibitory actions against the anabolic enzyme Akt or protein kinase B (Akt/PKB) (18, 22), an insulin-stimulated kinase that represses gluconeogenesis in the liver, increases glucose up-take in adipose tissue and muscle, and inhibits production of glucagon in pancreatic alpha cells. We found that exogenous ceramides, but not dihydroceramides, impaired insulin stimulation of the Akt/PKB enzyme in cultured hepatocytes (Fig. 4A) and adipocytes (fig. S11A) and that liver-specific ablation of *Degs1* enhanced activation of Akt/PKB in vivo (Fig. 4, B and C). By comparison, the ceramide effects on lipid metabolism result from several separable mechanisms that lead to increased uptake and storage of fatty acids in the liver and decreased mobilization and oxidation of fatty acids in adipose tissue. RNA sequencing (RNA-seq) experiments revealed that *Degs1* ablation dramatically lowered hepatic expression of sterol regulatory element binding transcription factor 1 (*Srebf1*), a master regulator of triglyceride and sterol production. *Srebf1* was the most highly down-regulated gene in $Degs1^{\delta Liver}$ knockout animals fed a NCD (Fig. 4D) and sixth most down-regulated gene in $Degs1^{\delta Liver}$ knockout mice maintained on a HFD (fig. S11B). Quantitative polymerase chain reaction (PCR) experiments confirmed that *Degs1* depletion decreased expression of *Srebf1* and several of its transcriptional targets (e.g., *Dgat1*, *Dgat2*, *Cidea*, and *Elovl1*) that encode proteins that enhance triglyceride storage (Fig. 4E). These data are consistent with prior studies showing that exogenous ceramides induce these targets in the liver (23). *Degs1* depletion inhibited fatty acid uptake into hepatocytes (Fig. 4F) owing to the ability of ceramides, but not dihydroceramides, to alter the subcellular distribution of the fatty acid translocase CD36 (Fig. 4G). *Degs1* depletion enhanced mitochondrial complex activity in adipose tissue (Fig. 4H), a finding that is consistent with our published data indicating that ceramides impair complex activity in adipocytes (20). We also found that ceramides, but not dihydroceramides, inhibit hormone-sensitive lipase (HSL) (Fig. 4, I to L), blocking the release of fatty acids from the triglyceride droplet. Prior published studies, together with our additional data, indicate that the ceramide effectors protein kinase Cζ or protein phosphatase 2A likely mediate the sphingolipid's effects on AKT (22, 24–27), *Srebf1* (28), CD36 (29), and HSL (Fig. 4, K and L).

The evolutionary basis for the ceramide actions described here is of interest. Why would cells respond to ceramides by shutting down insulin signaling while simultaneously activating a parallel pathway to enhance triglyceride accumulation? We surmise that ceramides serve as gauges of free fatty acid (FFA) excess when the energetic needs of the tissue have been met and the storage capacity (i.e., triglyceride synthesis pathway) is saturated. When this occurs, the excess fatty acids spill over into the sphingolipid synthesis pathway, producing ceramides and other sphingolipids that initiate cellular responses that prevent aberrant membrane dissolution by detergent-like FFAs. The following activities are consistent with this hypothesis: (i) Ceramides (and their product sphingomyelins) are key components of detergent-resistant membrane (DRM) domains that serve as scaffolds to support FFA diffusion (30–32). (ii) Ceramide induction of *Srebf1* increases expression of the enzymes that convert the incoming FFAs into triglycerides (e.g., DGATs) (Fig. 4E) and synthesize cholesterol, the key binding partner of ceramide and sphingomyelin in DRMs (33). (iii) Although FFAs can diffuse through cellular membranes (34–38), CD36 facilitates

their uptake and enhances their esterification (39, 40). By recruiting CD36 to DRMs (29), ceramides stimulate the conversion of FFAs into acyl–coenzyme A (CoA) to mitigate their detergent-like properties. (iv) Ceramide blockage of Akt/PKB inhibits the uptake and oxidation of glucose and amino acids (1, 6), leading to the preferential utilization of FFAs for energy. An ancillary benefit is that this inhibits the synthesis of new fatty acids. (v) Ceramide inhibition of lipolysis prevents liberation of additional fatty acids from the lipid droplet. (vi) Ceramide impairment of mitochondrial complexes decreases mitochondrial efficiency, enabling the cell to burn more fatty acids before maximally altering mitochondrial membrane potential. (vii) Ceramide synthases (CERS enzymes) respond to FFA by translocating to the nucleus, where they repress transcription of lipases (41, 42), thus providing an additional means by which the ceramide pathway decreases cellular FFA levels. Although this last action would be unaffected by *Degs1* depletion, the finding supports the supposition that the sphingolipid pathway's primary purpose is to protect the cell in times of FFA excess. We conclude that chronic elevation of tissue ceramides leads to persistent impairment in metabolic homeostasis, driving insulin resistance and hepatic steatosis.

This unifying theory provides an important framework for understanding how ceramides can elicit the entire spectrum of defects that underlie cardiometabolic disease. The idea also enables the development and testing of additional hypotheses regarding the regulatory events that control fuel utilization. For example, we predicted that β-adrenergic agonists, which liberate FFAs and enhance glucose utilization during times of stress, would decrease rates of ceramide production in order to release all of the energy stores during times of acute fuel need (e.g., by releasing fatty acids, activating Akt/PKB, and limiting triglyceride storage). Using the aforementioned flux method to quantify the incorporation of stable serine isotopes into the sphingoid backbone, we determined that the β-adrenergic agonist isoproterenol completely blocked ceramide biosynthesis in adipocytes (Fig. 4M).

Our data provide important resolutions regarding the relative contribution of ceramides versus dihydroceramides in the pathogenesis of metabolic diseases. Although in vitro studies have suggested that ceramides, rather than dihydroceramides, likely contributed to the inhibition of insulin signaling, several lipid profiling studies have identified dihydroceramides as particularly strong markers of metabolic dysfunction (7, 9). In particular, it has been reported that circulating dihydroceramides were strong prognostic indicators of future development of type 2 diabetes, appearing as early as 9 years before disease onset (8). We instead propose that dihydroceramides are not causative but likely serve as markers of increased flux of fatty acids through the biosynthetic pathway that produces the toxic ceramides. Our findings presented here indicate that ceramides contribute to metabolic disease and may offer an opportunity for clinical intervention.

Supplementary Material

Refer to Web version on PubMed Central for supplementary material.

ACKNOWLEDGMENTS

We are grateful for support from the Metabolomics, Histology, Genomics, and Metabolic Phenotyping Cores at the Health Sciences Center of the University of Utah.

Funding: The authors receive research support from the National Institutes of Health (DK112826 and DK108833 to W.L.H. and DK115824 and DK116450 to S.A.S.), the Juvenile Diabetes Research Foundation (JDRF 3-SRA-2019–768-A-B to W.L.H.), the American Diabetes Association (S.A.S.), the American Heart Association (S.A.S.), the Margolis Foundation (S.A.S.), and the USDA (2019-67018-29250 to B.C.). B.C. received a pilot grant from the Diabetes Research Center at Washington University in St. Louis of the NIH under award number P30DK020579. R.F.P. received a doctoral fellowship from FAPESP (process number 2014/17619–6). T.S.T. and J.L.W. received support from the NIH through the Ruth L. Kirschstein National Research Service Award 5T32DK091317. Studies conducted at Merck Research Laboratories in Kenilworth, NJ, were supported by Merck & Co., Inc.

REFERENCES AND NOTES

1. Chaurasia B, Summers SA, Trends Endocrinol. Metab 26, 538–550 (2015). [PubMed: 26412155]
2. Mamtani M et al., Obesity 22, 950–956 (2014). [PubMed: 23929697]
3. Brozinick JT et al., Int. J. Obes 37, 1064–1070 (2013).
4. Luukkonen PK et al., Diabetes Care 41, 1732–1739 (2018). [PubMed: 29844096]
5. Siddique MM, Li Y, Chaurasia B, Kaddai VA, Summers SA, J. Biol. Chem 290, 15371–15379 (2015). [PubMed: 25947377]
6. Bikman BT, Summers SA, J. Clin. Invest 121, 4222–4230 (2011). [PubMed: 22045572]
7. Summers SA, Cell Metab. 27, 276–280 (2018). [PubMed: 29307517]
8. Wigger L et al., Cell Rep. 18, 2269–2279 (2017). [PubMed: 28249170]
9. Luukkonen PK et al., J. Hepatol 64, 1167–1175 (2016). [PubMed: 26780287]
10. Anroedh S et al., J. Lipid Res 59, 1729–1737 (2018). [PubMed: 29858423]
11. Havulinna AS et al., Arterioscler. Thromb. Vasc. Biol 36, 2424–2430 (2016). [PubMed: 27765765]
12. Laaksonen R et al., Eur. Heart J 37, 1967–1976 (2016). [PubMed: 27125947]
13. Bergman BC et al., Am. J. Physiol. Endocrinol. Metab 309, E398–E408 (2015). [PubMed: 26126684]
14. Meikle PJ et al., PLOS ONE 8, e74341 (2013). [PubMed: 24086336]
15. Lemaitre RN et al., Diabetes 67, 1663–1672 (2018). [PubMed: 29588286]
16. Brockman HL et al., Biophys. J 87, 1722–1731 (2004). [PubMed: 15345551]
17. Omae F et al., Biochem. J 379, 687–695 (2004). [PubMed: 14731113]
18. Summers SA, Garza LA, Zhou H, Birnbaum MJ, Mol. Cell. Biol 18, 5457–5464 (1998). [PubMed: 9710629]
19. Holland WL et al., Cell Metab. 5, 167–179 (2007). [PubMed: 17339025]
20. Chaurasia B et al., Cell Metab. 24, 820–834 (2016). [PubMed: 27818258]
21. Brown MS, Goldstein JL, Cell Metab. 7, 95–96 (2008). [PubMed: 18249166]
22. Stratford S, Hoehn KL, Liu F, Summers SA, J. Biol. Chem 279, 36608–36615 (2004). [PubMed: 15220355]
23. Jiang C et al., J. Clin. Invest 125, 386–402 (2015). [PubMed: 25500885]
24. Bourbon NA, Sandirasegarane L, Kester M, J. Biol. Chem 277, 3286–3292 (2002). [PubMed: 11723139]
25. Powell DJ, Hajduch E, Kular G, Hundal HS, Mol. Cell. Biol 23, 7794–7808 (2003). [PubMed: 14560023]
26. Hajduch E et al., Biochem. J 410, 369–379 (2008). [PubMed: 17983354]
27. Blouin CM et al., Diabetes 59, 600–610 (2010). [PubMed: 19959757]
28. Taniguchi CM et al., Cell Metab. 3, 343–353 (2006). [PubMed: 16679292]
29. Xia JY et al., Cell Metab. 22, 266–278 (2015). [PubMed: 26190650]
30. Ehehalt R et al., BMC Cell Biol. 9, 45 (2008). [PubMed: 18700980]

31. Pohl J et al., Biochemistry 43, 4179–4187 (2004). [PubMed: 15065861]
32. Covey SD et al., Biochem. Biophys. Res. Commun 355, 67–71 (2007). [PubMed: 17291449]
33. Barenholz Y, Subcell. Biochem 37, 167–215 (2004). [PubMed: 15376621]
34. Pillai BK, Jasuja R, Simard JR, Hamilton JA, J. Biol. Chem 284, 33296–33304 (2009). [PubMed: 19801636]
35. Khan MA, Bishop RE, Biochemistry 48, 9745–9756 (2009). [PubMed: 19769329]
36. Brunaldi K, Huang N, Hamilton JA, J. Lipid Res 51, 120–131 (2010). [PubMed: 19625735]
37. Guo W, Huang N, Cai J, Xie W, Hamilton JA, Am. J. Physiol. Gastrointest. Liver Physiol 290, G528–G534 (2006). [PubMed: 16254047]
38. Hamilton JA, Johnson RA, Corkey B, Kamp F, J. Mol. Neurosci 16, 99–108 (2001). [PubMed: 11478390]
39. Jay AG, Hamilton JA, Prostaglandins Leukot. Essent. Fatty Acids 138, 64–70 (2018). [PubMed: 27288302]
40. Xu S, Jay A, Brunaldi K, Huang N, Hamilton JA, Biochemistry 52, 7254–7261 (2013). [PubMed: 24090054]
41. Chaurasia B, Holland WL, Summers SA, Trends Endocrinol. Metab 29, 597–599 (2018). [PubMed: 29685851]
42. Sociale M et al., Cell Rep. 22, 967–978 (2018). [PubMed: 29386138]

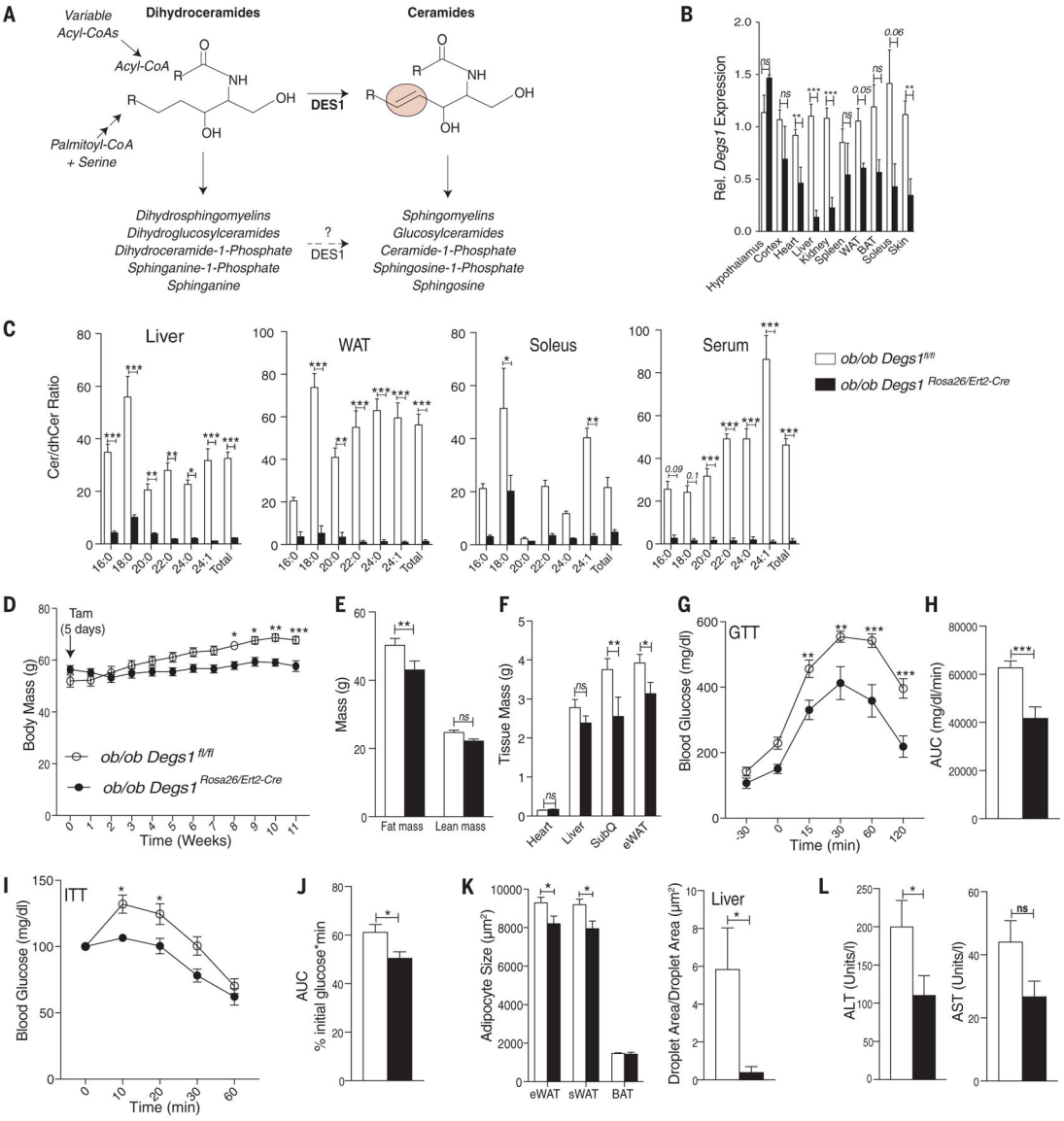

Fig. 1. Deletion of *Degs1* from leptin-deficient *ob/ob* mice improves glucose homeostasis and resolves hepatic steatosis.

(**A**) Schematic depicting the DES1 reaction. Dihydroceramides are produced through a biosynthetic pathway fueled by palmitoyl-CoA and serine, which produces the sphingosine backbone that subsequently incorporates additional fatty acids. DES1 then inserts the highly conserved 4,5-*trans* double bond into the sphingoid backbone. Both ceramides and dihydroceramides serve as precursors for the more predominant, complex sphingolipids. (**B** to **L**) Adult *ob/ob Degs1*$^{fl/fl}$ and *ob/ob Degs1*$^{Rosa26/ERT2\text{-}Cre}$ mice (20 weeks old) were injected with tamoxifen (3 mg) once daily over a 5-day time period. Animals were euthanized and tissues collected at 31 weeks of age. (B) *Degs1* mRNA expression and (C) ceramide/dihydroceramide ratios in tissues and serum; (D) body mass; (E) fat and lean mass when the animals were 30 weeks of age; (F) tissue mass; (G and H) glucose tolerance tests and area under the curve (AUC) when the mice were 23 weeks of age; (I and J) insulin tolerance tests and AUC when the mice were 24 weeks of age; (K) adipocyte size and liver

lipid droplet area; and (L) plasma ALT and AST levels. For each experiment, $n = 14$ to 16 mice per group were used, except for the hematoxylin and eosin staining used to calculate adipocyte and liver droplet size ($n = 3$ to 8 mice) or the AST/ALT determinations ($n = 7$ to 13 mice). Values are expressed as mean ± SEM, $*P < 0.05$, $**P < 0.01$, $***P < 0.001$ versus control. The “ns” denotes that the comparison was not significantly different. dhCer, dihydroceramide; Cer, ceramide.

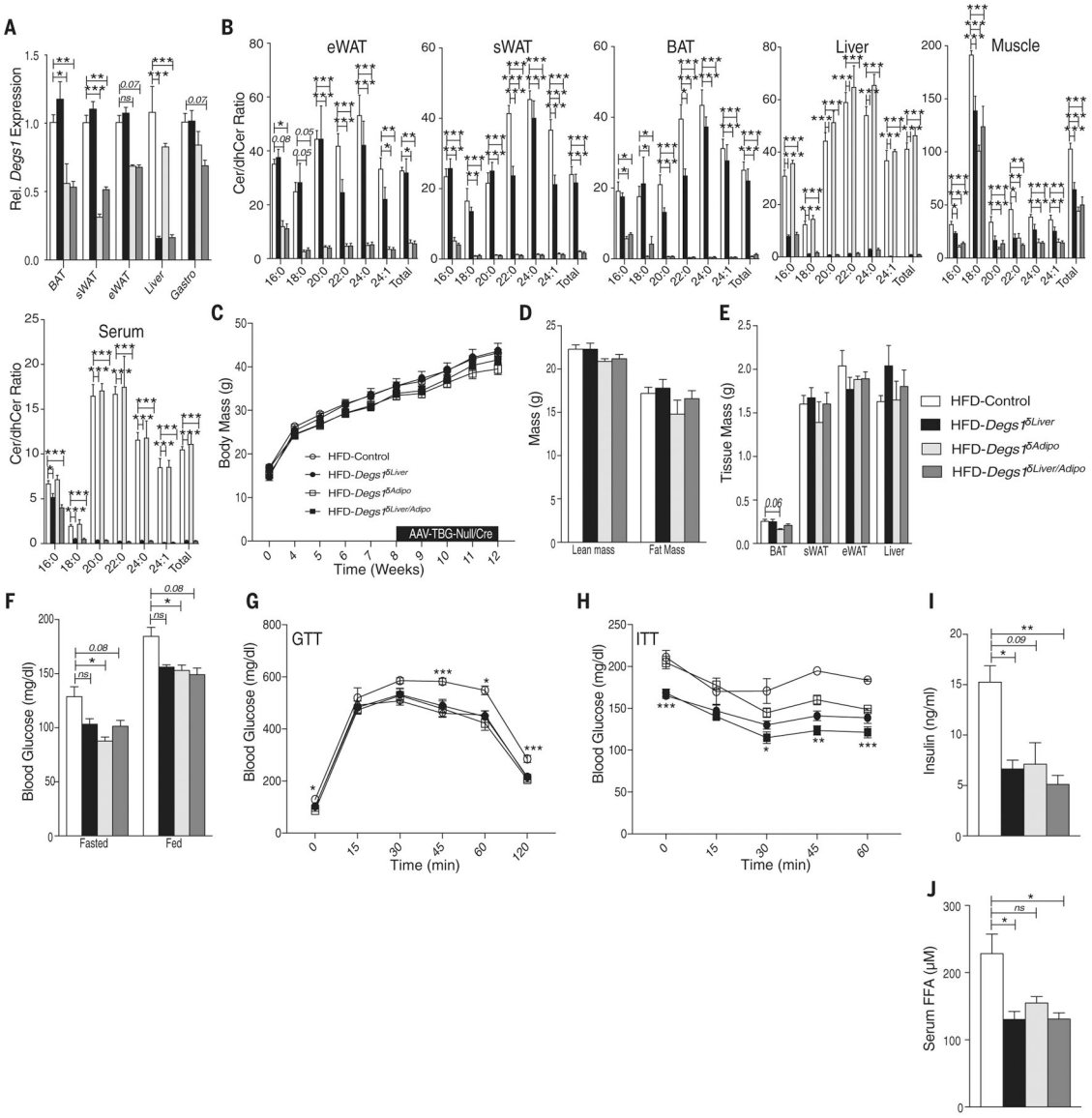

Fig. 2. Tissue-specific deletion of *Degs1* improves glucose homeostasis and resolves hepatic steatosis in mice.

(**A** to **J**) *Degs1*$^{\delta Adipo}$ or *Degs1*$^{fl/fl}$ littermate (control) mice were placed on a HFD at 4 weeks of age. At 12 weeks of age, *Degs1*$^{fl/fl}$ mice were injected with AAV-Tbg-Cre to produce *Degs1*$^{\delta Liver}$ or *Degs1*$^{\delta Liver/Adipo}$ mice (i.e., where *Degs1* is specifically deleted in the liver or liver plus adipose tissues, respectively). The other mice received control empty viruses (AAV-Tbg-Null). Euthanasia and tissue harvesting were performed when mice were 16 weeks of age. (A) *Degs1* transcript levels from indicated tissues; (B) ceramide/dihydroceramide ratios in tissues and serum; (C) body mass; (D) fat versus lean mass; (E) tissue mass; (F) fed and fasted blood glucose; (G) glucose tolerance tests were performed in animals when they were 14 weeks of age; (H) insulin tolerance tests were performed when they were 15 weeks of age; (I) serum insulin; (J) serum FFAs ($n = 3$ to 7 mice per group; replicate cohorts of animals were phenotyped separately, with the data included in figs. S3 to S7). Values are expressed as mean ± SEM, $*P < 0.05$, $**P < 0.01$, $***P < 0.001$ versus

control. eWAT, epididymal white adipose tissue; sWAT, subcutaneous white adipose tissue; BAT, brown adipose tissue.

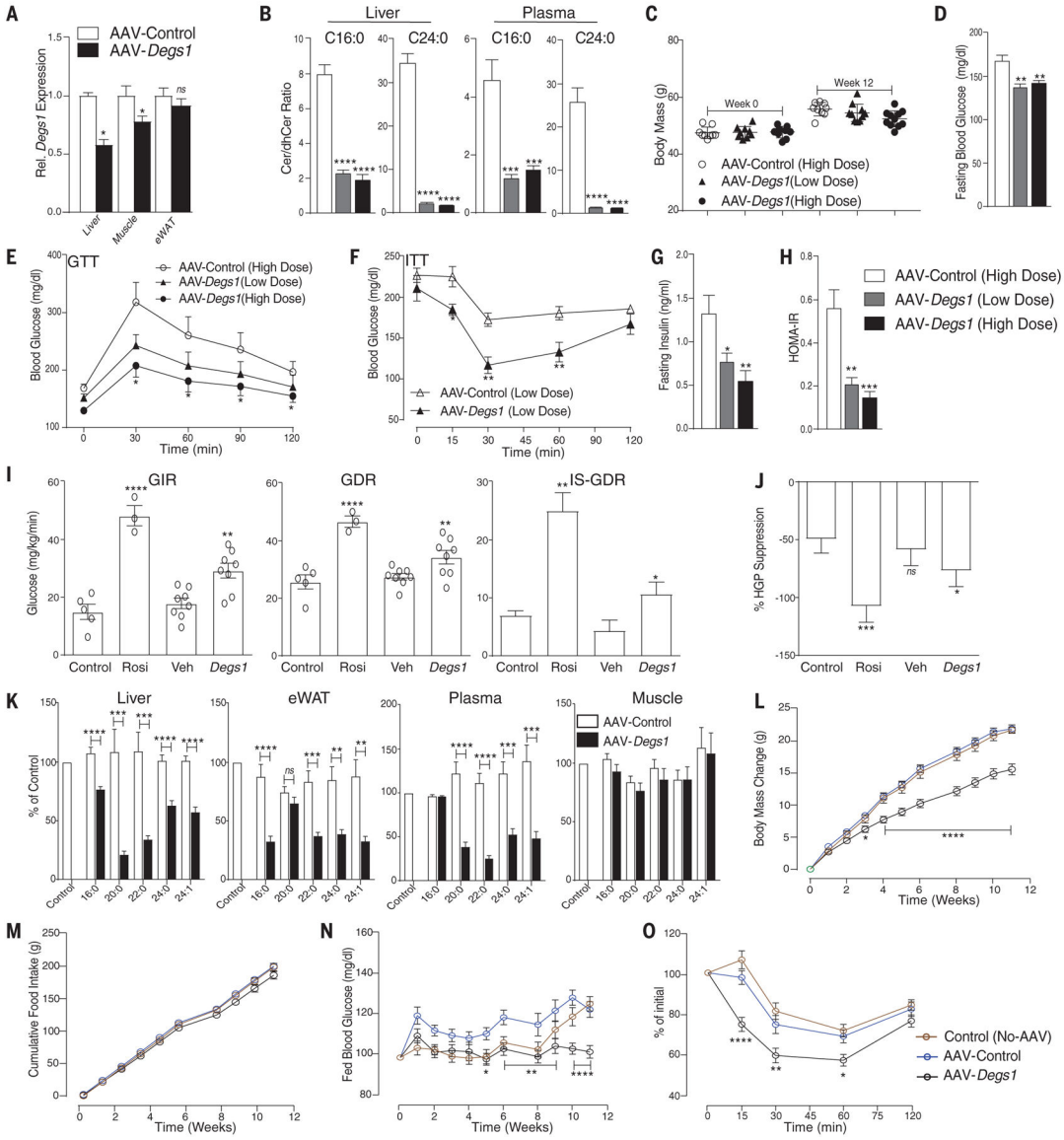

Fig. 3. Hepatic *Degs1* inhibition with AAV-*Degs1*-shRNA improves glucose homeostasis.

(**A** to **J**) Intervention study: 26-week-old C57BL/6 mice were placed on a HFD for 12 weeks. They were then injected with a single injection (1×10^{11} or 3×10^{11} genome copies/mouse, low dose or high dose, respectively) of AAV-*Degs1* expressing shRNA8 (AAV-*Degs1*) or a scrambled control (AAV-control). Mice were analyzed 12 weeks later. (A) Quantification of *Degs1* mRNA in the liver, eWAT, and muscle 12 weeks after administration of AAV-*Degs1*-shRNA or control; (B) liver and plasma ceramide/dihydroceramide ratios; (C) body mass; (D) fasting blood glucose; (E) glucose tolerance; (F) insulin tolerance; (G) fasting plasma insulin; (H) HOMA-IR; (I) glucose infusion rate (GIR), glucose disposal rate (GDR), insulin-stimulated GDR, and (J) hepatic glucose production. (**K** to **O**) Prevention study: 20-week old C57BL/6 mice were given a single injection (1×10^{11} or 3×10^{11} genome copies/mouse, low dose or high dose, respectively) of AAV-*Degs1* expressing shRNA8 (AAV-*Degs1*) or a scrambled control (AAV-control). They were then

placed on a HFD for 12 weeks. (K) Ceramide/dihydroceramide ratios in liver, adipose tissue, and plasma; (L) body mass; (M) food intake; (N) percent blood glucose change; and (O) insulin tolerance. $n = 10$ to 12 mice for both the intervention and prevention studies. Values are expressed as mean ± SEM, $*P < 0.05$, $**P < 0.001$, $***P < 0.0001$, $****P < 0.00001$ versus control.

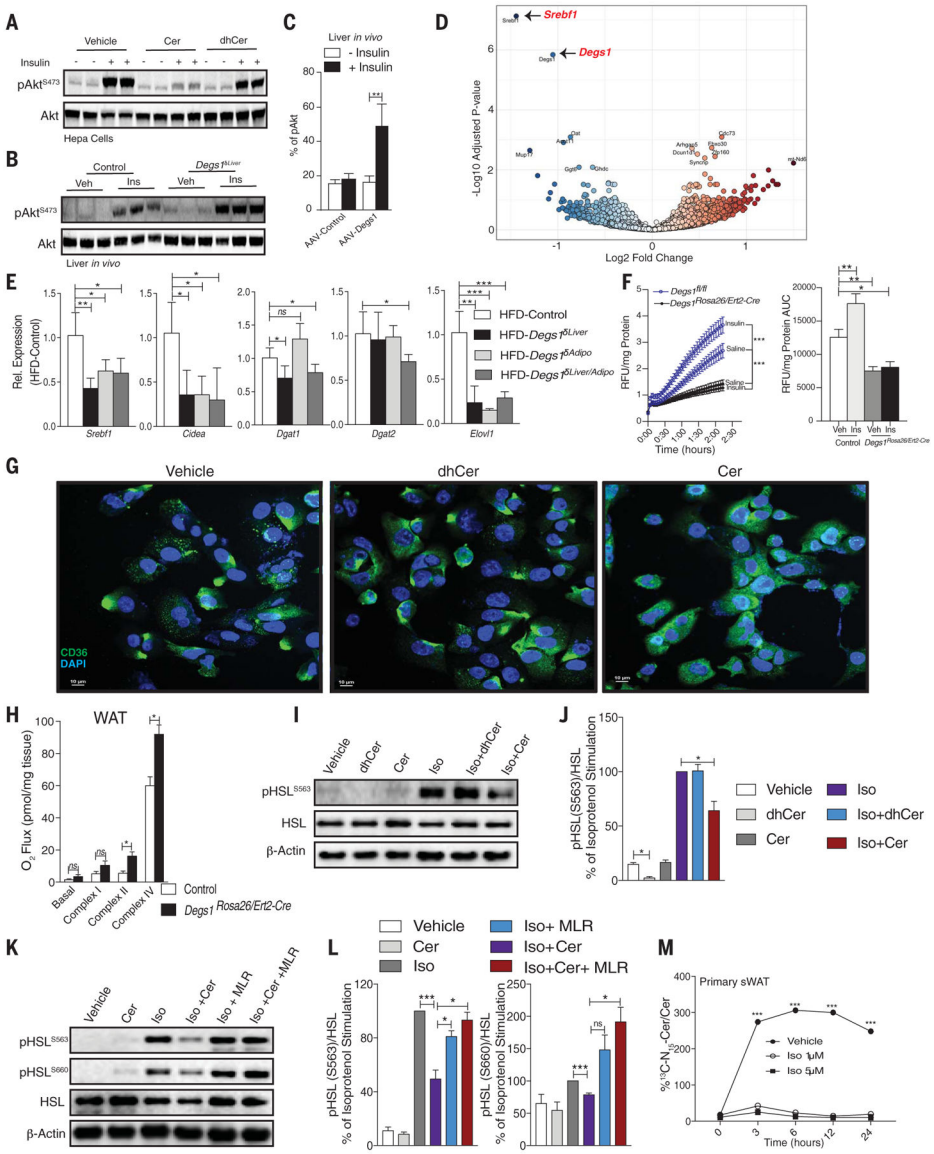

Fig. 4. Ceramides, but not dihydroceramides, induce selective insulin resistance.

(**A**) Hepa cells were treated with vehicle, C_2-ceramide (Cer), or C_2-dihydroceramide (dhCer) for 2 hours before stimulation with insulin (1 μM,10 min). Lysates were resolved by SDS-polyacrylamide gel electrophoresis, and Western blots were performed using antibodies recognizing phosphorylated Akt (p-Akt) or total Akt. (**B**) HFD-control and HFD-*Degs1*$^{\delta Liver}$ mice (as described in Fig. 1) were fasted for 5 hours before receiving a single dose of insulin (1 U/kg). The animals were euthanized 30 min later and tissues were flash frozen. p-Akt and Akt levels were determined by Western blotting as in (A). (**C**) C57BL/6 mice underwent the dietary and phenotyping regimen described for the intervention study (Fig. 3). Insulin stimulation of Akt/PKB phosphorylationwas determined by multiplex analysis (as described in the supplementary materials). (**D**) RNA-seq experiments were performed on livers from control and *Degs1*$^{\delta Liver}$ animals under chow-fed conditions. Similar RNA-seq data are presented in the supplementary materials (fig. S11B) for animals maintained on the HFD.

(**E**) Quantitative PCR determination of transcripts for SREBP-target genes in livers isolated from HFD-fed control, HFD-*Degs1*$^{\delta Liver}$, HFD-*Degs1*$^{\delta Adipo}$, and HFD-*Degs1*$^{\delta Liver/Adipo}$ mice ($n = 3$ to 5 per group, treatment regimen described in Fig. 2). (**F**) FFA uptake in primary hepatocytes isolated from control and *Degs1*$^{Rosa26/ERT2\text{-}Cre}$ mouse. (**G**) CD36 immunofluorescence in Hepa cells after treatment with either vehicle, Cer, or dhCer, as described in the supplementary materials. Scale bars, 10 μm. (**H**) Mitochondrial complex activity in WAT obtained from the control and *Degs1*$^{Rosa26/ERT2\text{-}Cre}$ mice maintained on a chow diet (2 weeks after receiving the five doses of tamoxifen). (**I**) Western blots depicting phosphorylated [pHSL(S563)] or total HSL in primary adipocytes treated with vehicle, Cer, C_6-dihydroceramide (dhCer), and/or isoproterenol (Iso), as described in the supplementary materials. (**J**) Quantification of pHSL(S563) from (I) ($n = 3$ independent experiments). (**K**) Western blots depicting Isoinduced phosphorylation of pHSL (S563 and S660 phosphorylation sites) after treatment with Cer for 4 hours and/or the PP2A inhibitor microcystin-LR (MLR) for 1 hour in primary adipocytes. (**L**) Quantification of pHSL (S563) and pHSL (S660) from (K) ($n = 4$ independent experiments). (**M**) Sphingolipid flux was determined by measuring the incorporation of L-serine-$^{13}C_3$,^{15}N into ceramide in primary adipocytes treated with Iso ($n = 4$). Values are expressed as mean ± SEM, $^{*}P < 0.05$, $^{**}P < 0.001$, $^{***}P < 0.0001$ versus control.